

Close stellar encounters kicking planets out of habitable zone in various stellar environments

Behzad Bojnordi Arbab,^{*} Sohrab Rahvar,[†]

Department of Physics, Sharif University of Technology, P.O. Box 11155-9161, Tehran, Iran

Accepted XXX. Received YYY; in original form ZZZ

ABSTRACT

Continuous habitability of a planet is a critical condition for advanced forms of life to appear, but it can be endangered by astronomical events such as stellar encounters. The purpose of this study is to analyze close stellar encounters able to change planetary orbits initially in circumstellar habitable zones, and to investigate the expected encounter rates in a variety of stellar environments. Using gravitational simulations for three-body systems, this study analyzed the dependencies of the encounter impact-parameters with kinematic, geometric and habitability parameters of the system. We also used kinematic properties of various stellar regions, and estimated encounter rates of the events. The expected number of threatening stellar encounters in the Solar neighborhood is $\approx 4 \times 10^{-4}$ in 4 billion years, while for Galactic bulge environment, we expect approximately six times the value. The encounter rates for other stellar environments are calculated and spheroidal dwarf galaxies and globular clusters encounter rates are estimated. The results shows that in contrast with the solar neighborhood, close stellar encounters can play a significant role in expected number of planets with continuous habitability in dense stellar environments. Further investigations are needed to study long-term multiple planetary systems and how it can change the overall expectation value of continuously habitable planets.

Key words: stars: kinematics and dynamics – planets and satellites: dynamical evolution and stability – Galaxy: general

1 INTRODUCTION

The search for other planets harboring life is one of the most ambitious projects in astronomy. As thousands of confirmed exoplanets are discovered in the recent years (NAS), the interest in finding habitable planets and eventually life-harboring planets increases. One of the main environments to search for life is the circumstellar habitable zone (CHZ or generally HZ, as used in this paper); the region around stars where a rocky planet in possession of an atmosphere can support liquid water. For a planet located in this region, life can potentially emerge, sustain and evolve (Huang 1959, 1960; Kasting et al. 1993; Kopparapu et al. 2013).

However, simply finding a planet in HZ is not a promise for life, as a sustained habitability is needed, and there might be catastrophic events threatening the existence of life on the planets. Various events originated from the planet can cause mass extinctions, for example, volcanic activities and eruptions causing catastrophic climate changes (Wignall 2001), as Several mass-extinctions have been characterized to be coinciding with mass-volcanism events (Alvarez 2003), with possi-

ble astronomical stimulations Pandey & Negi (1987); Abbott & Isley (2002).

Further than being a stimulant for terrestrial catastrophes, stellar encounters play a major role in many forms of ex-traterrestrial catastrophes. For instance, major-impacts of asteroids or comets can cause life-threatening catastrophes in a wide range of danger, from threatening many species to wiping out life from the face of Earth (Chapman & Morrison 1994). Almost all long-period comets come from the Oort cloud (Oort 1950), and due to perturbations, comets may inject into the inner solar system region. The outer Oort cloud radius is comparable to the distance of nearby stars and as a result, the gravitational force of a "stellar encounter" can induce a shower of comets into the inner planetary system, increasing major-impact rates (Hills 1981; Matese & Lissauer 2002; Wickramasinghe & Napier 2008). Bobylev (2017) studied the possible past and future stellar encounters from nearby stars that can produce the perturbations in the Oort cloud. Bailer-Jones (2017) utilized data from the first Gaia data release (GDR1) and other projects, and integrating the stellar motions through Galactic potential, identified close stellar encounters comparable to the Oort cloud. More recently, Bailer-Jones et al. (2018) implemented almost the same method for the second Gaia data release (GDR2). As a result of the gigantic size of the Oort cloud

^{*} E-mail: bojnordi_b._@physics.sharif.edu

[†] E-mail: rahvar@sharif.edu

and the weak binding of the cloud to the solar gravitation, other mass-encounters including the tidal force of the Galaxy and a dark matter disk (Rampino 2015), or giant molecular clouds (GMCs) (Mazeeva 2004; Jakubík & Neslušan 2008) can perturb Oort cloud enough to alter the rate of comets falling in the inner regions of solar system. Moreover, GMC encounter can increase the influx of cometary dust (Hoyle & Lyttleton 1939; Shaviv 2003).

In recent years, many astronomers studied stellar encounters for different reasons and in various scenarios, including planetary ejections and rogue planets, interactions with circumstellar protoplanetary disks, and perturbations on the Oort cloud or on planetary orbits. As for one of the first attempts for calculating the effects of stellar encounters, Lyttleton & Yabushita (1965) calculated the changes in planetary orbital parameters from a passing star by the method of variation of elements, and also took into account the cumulative effects of multiple encounters. One of the early motivations to study such encounters came from primitive predictions (e.g. Rasio & Ford (1996)) and observations (e.g. Luhman et al. (2005)) of rogue planets. In an attempt to calculate the number of rogue planets in star clusters, Hurley & Shara (2002) performed N-body simulations for the M22 cluster, and taking into account the interactions between a set of Jupiter-mass planets and the nearby cluster stars, calculated the percentage of planets ejected by the encounters, and the fraction that leave the cluster afterward. Veras & Raymond (2012) also showed that the planet-planet interactions can not explain the majority of rogue planets alone, so the stellar encounters can be responsible for the remaining bulk.

In the early formation-period of a planetary system, stellar encounters can be critical in the properties of later protoplanetary disks and the planetary system. Kobayashi & Ida (2001) investigated the changes in eccentricity, inclination, and longitude alignments of the protoplanets in inner and outer regions of protoplanetary disks, caused by an encounter event. Stellar encounters can also change the density profile and shrink the size of protoplanetary disks. Vincke et al. (2015) investigated the truncation of the disks in different cluster populations, showing that in birth clusters like Orion Nebula Cluster, stellar encounters play an important role in shaping the protoplanetary disks. We can also expect star capture (Clarke & Pringle 1991), ejection of disk matter, or an angular momentum transfer to the star (Hall et al. 1996; Ostriker 1994). Stellar encounters in young clusters can strip stars of debris disks (Lestrade et al. 2011), change eccentricity, capture or send the planets out of the planetary system (Li & Adams 2015; Malmberg et al. 2011; Jiménez-Torres et al. 2011). However, the consequences of stellar encounters can be altered or canceled through dynamical processes of later planetary formation stages. Marzari & Picogna (2013) and Picogna & Marzari (2014) showed that the circumstellar disk can erase the stellar encounter effects on protoplanets eccentricities in ≈ 10 kyr during the stay in the birth cluster, but the semi-major axes do not revert to the initial sizes. Portegies Zwart & Jílková (2015) distinguished the circumstellar regions in open clusters based on gravitational effects from external and internal planetary system influences by defining Parking Zone and Frozen zone. These zones specify the size of the circumstellar orbital space mainly uninfluenced by stellar encounters. Incidents of stellar encounters in dense clusters changes the population of planets and plays an important

role in planetary formation procedures (Jiménez-Torres et al. 2011; Fagner & Nelson 2009; Craig & Krumholz 2013; Malmberg et al. 2011).

Another motivation to study stellar encounters has been the rate of cometary impacts through the history of the Earth, and how stellar encounters can affect the number of comet orbits reaching the inner parts of solar system, and eventually changing the impact rates from comets. Rickman et al. (2008) studied the effect by modeling an Oort cloud and random stellar encounters to measure the impact of stellar and cometary orbital parameters on injections of comets into inner solar system. Feng & Bailer-Jones (2014) extended the model to study the variations of long-period comets with regard to gravitational perturbation from galactic tide and stellar encounters. Inspired by these results, Martinez-Barbosa et al. (2016) took into account different galactic orbits of solar system, and how it can change the rate of stellar encounters that can effectively interact with the Oort cloud, considering stellar encounters within $10^5 AU$ from sun.

As stated above, the role of stellar encounters in ejection of planets is discussed (e.g. Lyttleton & Yabushita (1965); Veras & Raymond (2012); Portegies Zwart & Jílková (2015); Cai et al. (2017); van Elteren et al. (2019)), but in this work, we specifically focus on the persistence of the planetary orbit in the "habitable zone" due to the encounters, especially for the case of planets in Earth-like orbits. Also, we used the time-scale of life on Earth to study the chances of stellar encounters that can endanger the continuously habitability of the planet. We present results in the solar neighborhood, Galactic bulge, birth clusters, globular clusters and spheroidal dwarf galaxies. The informations on the effectiveness of such encounters on changing the habitable orbits out of their habitable zone identifies the environments that this effect should be taken into account and how it can change our expectations on the number of planets harboring life in different regions.

Note that we use a simplified close stellar encounter catastrophe; the changes in other planetary orbits and the interplanetary gravitational effects are yet to be studied. The addition of other planets and taking into account the interplanetary interactions makes the simulations much more expensive. Therefore, we introduce "one percent chance encounter rate" to compare different environments in the matter of such encounter rates.

This paper is organized as follows. In section (2), we express the methods used for simulating the close stellar encounters, defining the critical impact-parameter and cross-section, threatening impact parameter and cross-section, and threatening encounter rate. In section (3), we study the correlations between the critical impact parameter, the initial parameters of the encountering star, and the habitable zone width, and finally, calculate the critical encounter rates for the solar system neighborhood and the Milky Way bulge. The conclusion is given in section (4)

2 METHODS AND DATA

In this section, we begin by introducing the close stellar encounter and associated parameters. Also, we discuss the rate of encounters that can deviate the planet's orbit from the habitable zone.

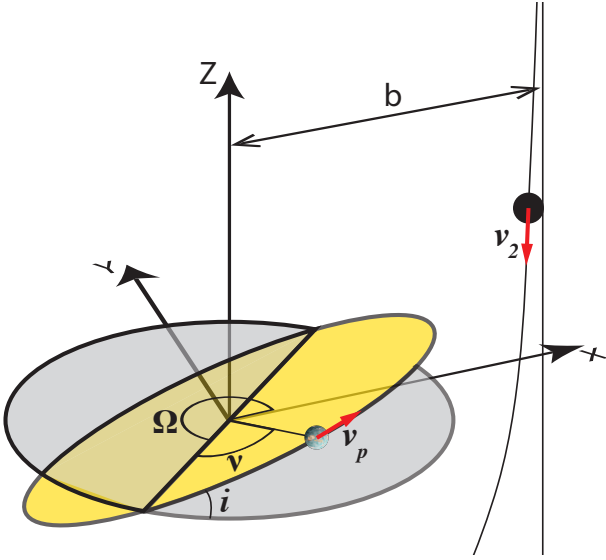


Figure 1. The orbital parameters of encounters is as follows: b is the impact parameter of the secondary star with respect to the parent star, v_2 is the initial velocity of the secondary star, v_p is the initial orbital velocity of the planet, Ω is the longitude of the ascending node, i is the inclination of the planetary orbit with respect to the (x-y) plane and ν is the initial anomaly of the planets measured counterclockwise from the ascending node.

2.1 Methods

For simplicity, we assume a gravitational system consisting of three bodies: (i) the parent star, (ii) the orbiting planet around the parent star, and (iii) the encountering star. We simplify the physics of encountering by assuming that the target star has one planet, where together with the encountering star, makes a three-body gravitational interaction. For the encountering stars, we use the kinematic and the stellar population of stars in Galaxy while we adapt the target star as a solar-type star and the planet as an Earth-type planet (García-Sánchez et al. 2001). Here for simplicity, we ignore the encountering binary and multiple stars.

For the numerical calculation, we use the gravitational integrations for the stellar encounter by the REBOUND code¹ (Rein & Liu 2011) and the IAS15 algorithm (Rein & Spiegel 2014), which is a 15th-order gravitational dynamics integrator and optimized for integrating close-encounter schemes. The encountering parameters in our study are (i) the velocity and mass of the encountering star (v_2 and M_2), (ii) the impact parameter of the encountering star with respect to the primary star (b), (iii) two angular parameters indicating the orientation of the planetary orbital plane with respect to the encountering star (i.e., Ω and i in Figure 1) and (iv) the initial anomaly of the planet (i.e., ν in Figure 1). We also have a parameter indicating the width of the habitable zone (W_{hz}). Here, we adopt the mass of the parent star to be one solar mass and the planet to be a test particle.

We place the origin of the Cartesian coordinate system on the position of the parent star. The secondary star is initially at the position of $(x, y, z) = (b, 0, 50\text{AU})$, along the z axis in this coordinate. Two angular parameters are required to

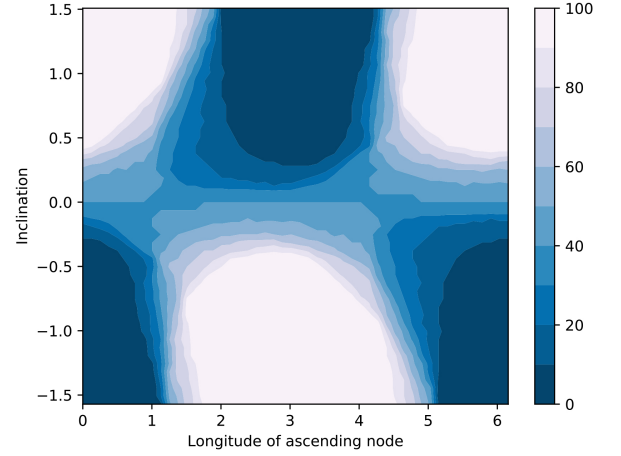


Figure 2. Probability function of the planetary orbit that remain in the habitable zone in percent. Here we adapt $M_2 = 1M_\odot$, $v_2 = v_p$ and $b = 4a_p$, the the primary system is identical to the sun-earth parameters, Kasting et al. (1993) conservative instantaneous HZ is used, and the percentage is calculated from a pool of initial anomaly of the planet. Both inclination and longitude of ascending node are measured in radians.

specify the initial alignment of planet orbit in this coordinate system; the inclination angle of " i " from the xy plane and the longitude of the ascending node (Ω) of the planetary orbit which is measured from the x -axis. Also, we measure the anomaly of the planet (i.e., ν) from the ascending node, counterclockwise on the planet's orbital plane.

In our simulation, we scan all the mentioned parameter space with the following range of $\Omega \in [0, 2\pi]$, $\nu \in [0, 2\pi]$, $i \in [-\pi/2, \pi/2]$, $b \in [0.1, 100]a_p$ where a_p is the planet orbital radius. All the parameters are chosen with uniform distribution functions. The kinematic parameters such as v_2 and the mass of the secondary star, M_2 have their own distribution functions and will be discussed in the next section. For each run of the simulation, the initial parameters are selected from the mentioned 6-dimension space and finish the calculation of the dynamics when the encountering star reaches the distance of $z = -50$ AU far from the primary star. After the encounter, we calculate the orbital parameters of the planet.

2.2 habitable-zone expelling/safe encounters and critical impact parameter

An event is a "habitable-zone expelling encounter" if perturbations from the encountering star push the planet out of the habitable zone via the inner or outer boundaries of HZ, or is a "safe encounter" if it stays in the HZ after the encounter. In each encounter, the total numerical relative energy error is less than $\Delta E/E < 10^{-14}$, and the total numerical relative angular momentum error is less than $\Delta L/L < 10^{-15}$. Note that the habitable-zone expelling encounter, by definition, is just about a specific impact parameter and does not say anything about smaller impact parameters, but evident from Figure 3, one can conclude that in larger impact parameters, the encounters will be safe ones.

Figure 2 demonstrates an example from our simulation where we fix three parameters of M_2 , v_2 and b . Here v_p is

¹ <https://rebound.readthedocs.io>

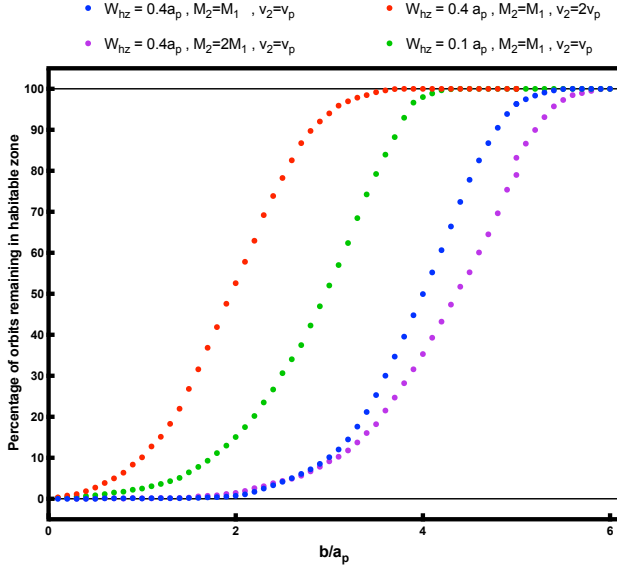


Figure 3. Percentage of orbits remaining in the habitable zone for different initial conditions.

the orbital velocity of the planet around the parent star. In this figure, we identify stellar encounters in terms of Ω versus i integrated over all the values of anomalies. The mean percentage over the plot shows the probability function for the planet remaining in the habitable zone of the parent star (P_{HZ}). The probability function for the planet exiting the habitable zone is clearly $1 - P_{HZ}$.

In what follows, we classify the parameters of this problem into two groups as (M_2, v_2, b, W_{hz}) and the second group identifying the angular orientation of the planet as $(i, \Omega$ and $\nu)$. We will integrate over the parameters in the second group to provide the probability function of a planet remaining in the HZ (i.e., P_{HZ}), in terms of the first group of parameters. Figure (3) represents another example from our simulation where we calculate P_{HZ} as a function of impact parameter for various sets of the mass and the velocity of encountering stars and the width of the habitable zone. As shown in Figure (3), we define the "critical impact parameter" (b_c) as the smallest impact parameter where P_{HZ} is 100%.

We study the relationship between the critical impact parameter (b_c) and physical parameters such as the width of the habitable zone boundary (W_{hz}), velocity (v_2) and mass (M_2) of the encountering star, integrating over the rest of the parameter space. Here we simulate 8000 encounters for each set of physical parameters and scanning uniformly over i , Ω , and ν .

2.3 Threatening encounter rate

In order to measure the rates of encounters that are threatening to the habitability of the planet, we should use an average value of HZ expelling/safe probabilities over cross-section elements. The value requires a probability-threshold, which we choose it to be 1%, and call it the Threatening cross-section (σ_T): "the cross-section around the primary star, where encounters within have 1% probability for the planet to exit HZ (a HZ expelling encounter happens)".

To calculate the threatening cross section, we integrate in

the impact-parameter space over probability function of HZ expelling encounters:

$$\frac{\int_0^{b_t} 2\pi b(1 - P_{HZ})db}{\pi b_T^2} = 1\% \quad (1)$$

$$\sigma_T = \pi b_T^2 \quad (2)$$

We note that the cross-section is a function of velocity and the mass of the secondary star and the width of the habitable zone. We can calculate the "Threatening Encounter Rate" (Γ_T) as the rate of flybys within the σ_T , which can be evaluated by: (Hut & Tremaine 1985; García-Sánchez et al. 2001; Li & Adams 2015)

$$\Gamma_T = n_* \langle \sigma_T \rangle_{(v)} \sqrt{v_\odot^2 + v_*^2}, \quad (3)$$

where v_\odot is the peculiar velocity of the sun in local standard of rest in the solar neighborhood (Bobylyev & Bajkova 2014), v_* is the velocity dispersion of stars, n_* is the number density of the stars in the environment, and $\langle \sigma_T \rangle_{(v)}$ is the averaged threatening cross-section over the stellar velocities function in the environment $f_{(v)}$. We assume a Maxwell Boltzmann velocity distribution function, where:

$$f_{(v)} = \sqrt{\frac{2}{\pi}} \frac{v^2 e^{-\frac{v^2}{2\alpha^2}}}{\alpha^3}, \quad (4)$$

where α is the scale parameter, which has the following relationship with the velocity dispersion:

$$v_* = \sqrt{\frac{\alpha^2(3\pi - 8)}{\pi}}, \quad (5)$$

therefore, the probability density function with regard to the velocity dispersion is:

$$f_{(v)} = \frac{\sqrt{2(3\pi - 8)^3}}{\pi^2 v_*^3} v^2 e^{-\frac{(3\pi - 8)v^2}{2\pi v_*^2}}. \quad (6)$$

As a result, the threatening encounter rate (Γ_T) is specific for each stellar mass and corresponding velocity dispersion.

3 RESULTS

In this section, we present the underlying aims of the research. We study the relationship between the critical impact parameter with the physical parameters (i.e., the velocity and the mass) of the encountering star. Then, the relation of the critical impact parameter with the width of the habitable zone for various ranges is studied. We also study the effect of the inclination angle of the orbital plane of the planet on HZ expelling encounters. This section concludes by presenting the results for Threatening cross-section and threatening encounter rates for various stellar environments. We also present the total threatening encounter rate and the probability of such encounters in the 4-billion years period. We use Kasting et al. (1993) conservative definition of instantaneous HZ (and we call it Kasting HZ) throughout this paper, unless indicated otherwise.

3.1 Dangerous impact parameter relation with encounter parameters

3.1.1 The relation between the critical impact parameter and the velocity of the secondary star

In order to investigate the relationship between the critical impact parameter and the initial velocity of the encountering star, we simulated systems with a broad range of velocities compare to the dispersion velocity of stars. In Figure (4), we plot the critical impact parameter normalized to the orbital radius of the planet, as a function of the relative velocity of encountering star with respect to the velocity of the planet. Here we have different scaling relation of the power of ~ -1 for the small and power of ~ -0.5 for the large velocities of the encountering stars.

We can interpret Figure (4) from the rough analysis of the gravitational impact. Let us use the generic relation between the minimum encounter distance (i.e., r_{min}) and impact parameter (i.e., b) (Hills 1984) from the three body problem as follows

$$r_{min} = a_c \left(\left[1 + \left(\frac{b}{a_c} \right)^2 \right]^{1/2} - 1 \right), \quad (7)$$

where

$$a_c = \frac{G(M_1 + M_2)}{v_2^2}, \quad (8)$$

and a_c is the accretion radius, parameterizing the gravitational focusing.

High velocity regime: In the case of a distant encounter and high relative velocities ($v_2 \gg v_p$) the gravitational impulse (ΔI) at the given distance from the star is proportional to (Martínez-Barbosa et al. 2017)

$$\Delta I \propto \frac{M_2}{v_2 r_{min}^2}. \quad (9)$$

For the high velocities of encountering star, from the combination of equation (7) and equation (8), we can conclude that r_{min} is almost equal to the impact parameter, b . As a result from equation (9) for a given impulse, to push the planet out of the habitable zone,

$$b_d \propto v_2^{-0.5}. \quad (10)$$

The high-velocity HZ expelling encounters of stellar masses lower than $1M_{\odot}$ occur with approximately asteroid belt distances.

Low velocity regime: For the low relative velocities of the two stars (i.e., $v_2 < v_p$), from equation (7), $r_{min} = \frac{1}{2} \frac{b^2}{a_c}$ where substituting the definition of a_c from equation (8) results in

$$b_d \approx \frac{[2r_{min}G(M_1 + M_2)]^{1/2}}{v_2}. \quad (11)$$

So the critical impact parameters related to the initial velocity of the secondary star as $b_d \propto v_2^{-1}$. It means that we see the gravitational lensing in the encountering star flyby in low relative velocity, but not in high velocities. Such encounters happen in distances comparable to Uranus and Pluto orbital radii.

The critical impact parameter as a function of the low and high velocity regimes of the secondary star is consistent with Figure (4).

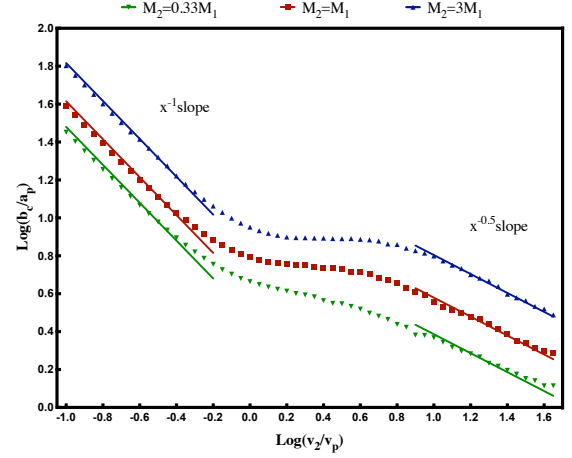


Figure 4. The critical impact parameter normalized planetary orbital radius, as a function of the relative velocity of the encountering star with respect to the velocity of the planet, both in logarithm scales. The three datasets are for different secondary star masses; $M_2 = 0.3M_1$, $M_2 = M_1$, $M_2 = 3M_1$, and Kasting HZ is used. Logarithm bases are 10. The limits are chosen to demonstrate the changeover.

3.1.2 Relation between the critical impact parameter and the mass of the secondary star

The relative mass of the secondary star to the primary star (i.e., M_2/M_1) plays a significant role in the size of the critical impact parameter. We performed simulations for the relative mass in the range of $0.1 < M_2/M_1 < 10$. The results of our simulation are represented in Figure (5) for the impact parameter in terms of the relative masses for three different velocities of the secondary star. By increasing the mass of the secondary star, the tidal forces on the star-planet system increases, and the critical impact parameter occurs in the larger distances.

Fitting the numerical results with a power-law function results in

$$\frac{b_d}{a_p} \propto \left(\frac{M_2}{M_1} \right)^{0.34}. \quad (12)$$

This equation is almost similar to the Hill radius, $r_H \propto (M_2/M_1)^{1/3}$, which represents the unstable sphere around the primary star in the binary system. However, we note that in the Hill radius $M_2 \ll M_1$, unlike to the system in our concern. Also, b_d is the impact parameter of the encounter, rather than the minimum distance of the stars. In our notation, the mass-ratio is the inverse of mass ratios in Hill's problem, as M_1 is the and M_2 are Sun and the small planet, but here the orbit is around M_1 , and the star with M_2 is passing. The orbital radii is inversed too, therefore the overall relations are still alike, but the $1/3$ slope in log-log plot occurs in high mass-ratios.

3.1.3 Relation between the critical impact parameter and width of the habitable zone

In the previous sections, we have used a fixed habitable zone boundary. The HZ around the sun depends on the criteria on the planetary climate models. Hart (1979) calculated the

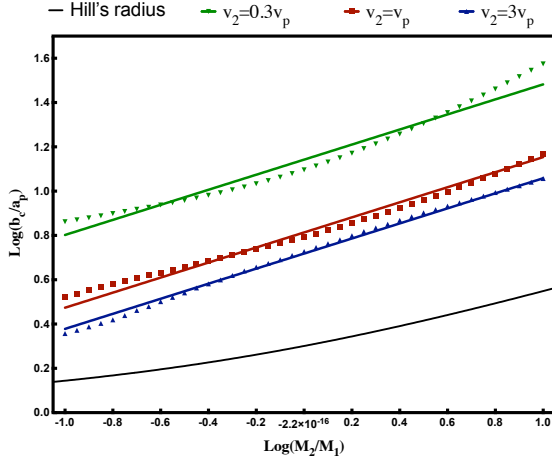


Figure 5. Log-Log plot of the critical impact parameter as a function of the mass of the secondary star, relative to the primary star for three different velocities. plotted for three different velocities: $v_2 = 0.3v_p$, $v_2 = v_p$ and $v_2 = 3v_p$. The black curve is the Hill's radius without the negligible mass or orbital radius assumption. Note that here the 1/3 slope occurs in higher mass ratios. Kasting HZ boundaries are used.

inner and outer boundary to be 0.95 au and 1.01 au, respectively. Kasting et al. (1993) identified conservative instantaneous HZ to be between 0.95 au to 1.37 au, conservative continuous HZ to be 0.95 au to 1.15 au, and optimistic instantaneous habitable zone to be in the 0.84 au to 1.67 au, respectively. Kopparapu et al. (2013) also estimated the HZ boundaries to be 0.99 au and 1.70 au. In this section, we let the habitable width to be a free parameter and study the critical impact parameter in terms of the width of the habitable zone.

In the simulations, we adopt the position of the planet to be in the median radius of the habitable zone. The result of our simulation is shown in Figure (6) for three different mass-ratios and two different initial velocities of the secondary star. The scaling relation between the critical impact parameter and the width of the habitable zone is a power-law function as $b_d \propto W_{hz}^\beta$ where $\beta < 0$ and it is a function of the stellar mass ratio (M_2/M_1) and the initial velocity of the secondary star (v_2). We note that W_{hz} depends on the stellar type and a model we are adapting for the habitable zone. In our study, we take a solar-type parent star. Our results show that the rate of HZ expelling encounters has a small dependence on the definition of the habitable zone model.

3.2 The most threatening orbital inclinations for the encounters

Different inclinations of the planet orbit with respect to the orbital plane of the secondary star changes the ratio of HZ expelling encounters. In order to study the probability function for the HZ expelling encounters, we simulated planets with a fixed initial inclination angle and an impact parameter and change the initial anomaly and longitude of ascending node. We integrate over the nuisance parameters (i.e., ν and Ω) and calculate the ratio of events where the planet remains in the habitable zone for each set of inclination and impact parameter, as shown in Figure (7). For a given impact parameter,

Table 1. Populations of stars in the solar neighborhood, with velocity dispersion (in km/s), peculiar velocity of sun (in km/s), mass (in solar mass), and stellar number density (in $10^{-3}pc^{-3}$). Stellar types include MK types for main-sequence stars, white dwarves (WD), and giants. (The data is adapted from Table 8 of García-Sánchez et al. (2001))

Stellar type	v_* (km/s)	v_\odot (km/s)	$M(M_\odot)$	$n_*/pc^3 \times 10^{-3}$
B0	14.7	18.6	18	0.06
A0	19.7	17.1	3.2	0.27
A5	23.7	13.7	2.1	0.44
F0	29.1	17.1	1.7	1.42
F5	36.2	17.1	1.3	0.64
G0	37.4	26.4	1.1	1.52
G5	39.2	23.9	0.93	2.34
K0	34.1	19.8	0.78	2.68
K5	43.4	25.0	0.69	5.26
M0	42.7	17.3	0.47	8.72
M5	41.8	23.3	0.21	41.55
WD	63.4	38.3	0.9	3.00
Giants	41.0	21.0	4	0.4

a critical impact depends on the inclination angle where for large impact parameters, larger inclination (almost parallel to the planetary orbit) are more dangerous and for the small impact parameter the smaller inclinations (almost perpendicular to the planetary orbit) are the dangerous encounters. Averaging over the impact parameters, the percentage of planets remaining in HZ is not sensitive to the inclination angle.

3.3 Threatening encounter rates in various stellar environments

From evidence found in old hydrothermal vents, life on earth has been existed for about 4 billion years (Dodd et al. 2017). For a planet in habitable zone of a Solar-type star in order to maintain life like the present Earth, we assume that the planet should be safe for at least 4 billion years.

3.3.1 Solar neighborhood

Data: We use data of the populations of stars in the solar neighborhood from Rickman et al. (2004), Allen (1973) and García-Sánchez et al. (2001) to calculate threatening encounter rates for each stellar population as shown in Table 1.

Results: Using equation (3), we calculate in Table 2 the cross-sections and rates of the threatening encounters for each population listed in Table 1. The overall threatening encounter rate is $1.09 \times 10^{-4} Gyr^{-1}$, where for a period of four billion years, the encounter probability is 4.35×10^{-4} . We would expect to have at least one threatening encounter out of ≈ 2300 planets in habitable orbits.

3.3.2 Bulge of Milky Way galaxy

Data: Wegg & Gerhard (2013) used the Red Clump Giants (RCGs) from the vvv survey (Saito et al. 2011) and calculated the 3-dimensional density distribution of bulge within

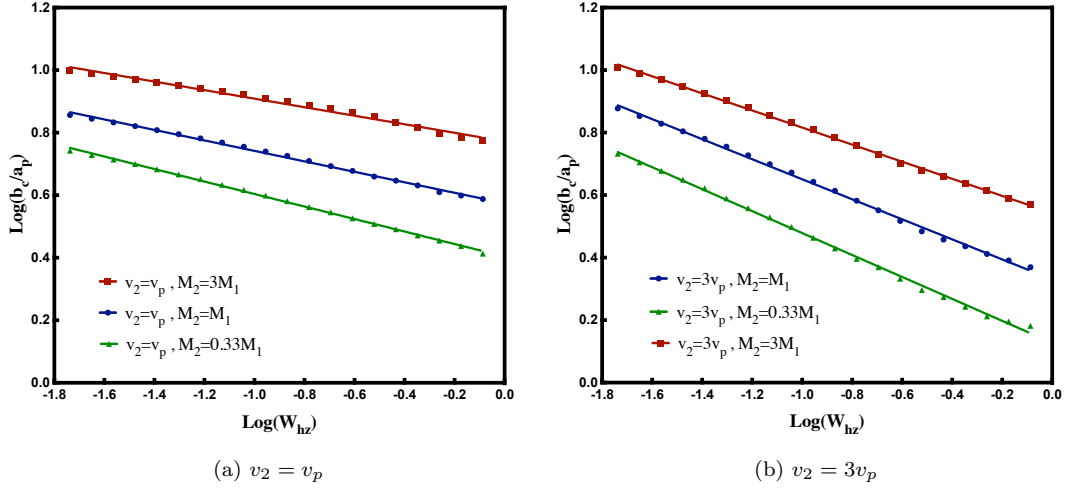


Figure 6. The critical impact parameter in logarithmic scale as a function of W_{hz} in logarithmic scale with three different M_2 values. The two figures differ in the velocity of the encountering star (v_2). As shown, the relationship between critical impact parameter and W_{hz} is a power law (linear in Log-Log plot), with different powers, depending on v_2 and M_2 . We interpret the dependence of critical impact parameter to M_2 in equation (12).

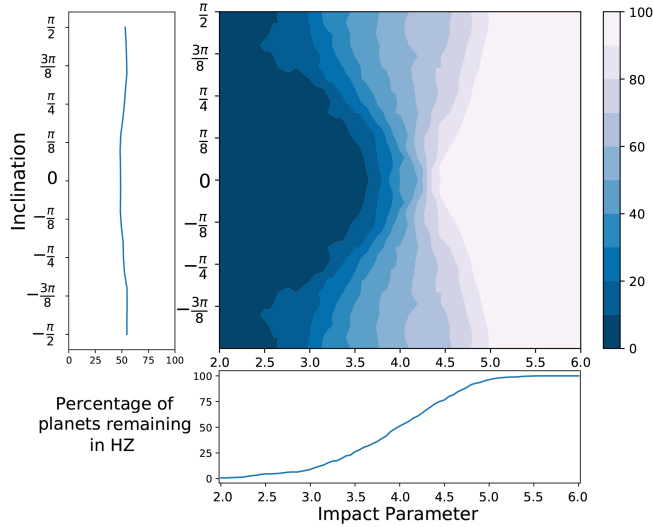


Figure 7. The ratio of events that the planet remains in the habitable zone, as a function of the inclination angle of the planetary orbital plane, and the impact parameter. For impact parameters in the range of $b/a_p < 2$, a hundred percent of events are HZ expelling encounters, and for $b/a_p > 6$, none of the encounters are HZ expelling. Here, we have integrated over the initial anomalies and longitude of ascending node of the planetary orbit. The HZ boundaries used are 0.8-1.2 AU.

the volume of $(\pm 2.2 \text{ kpc} \times \pm 1.4 \text{ kpc} \times \pm 1.1 \text{ kpc})$ surrounding the Galactic center. On the other hand, Portail et al. (2015) created a dynamical model using Wegg & Gerhard (2013) RCGs density measurements and velocity distribution data from Bulge Radial velocity Assay (BRAVA) spectroscopic survey (Rich et al. 2006; Howard et al. 2008; Kunder et al. 2012) and evaluated the stellar mass of the inner Galactic bulge region to be $1.25 - 1.6 \times 10^{10} M_\odot$. From the volume of the bulge and the stellar mass, we estimate the mean stellar-mass density to be $\approx 0.5 M_\odot/\text{pc}^3$.

Table 2. The threatening encounter cross-sections (in the unit of AU^2 and threatening encounter rate (in the unit of Gyr^{-1}) for the stars listed in Table 1.

Stellar type	$\langle \sigma_T \rangle (\text{AU}^2)$	$\Gamma_d (\text{Gyr}^{-1})$
B0	5.11×10^4	1.74×10^{-6}
A0	1.18×10^4	2.00×10^{-6}
A5	8.22×10^3	2.38×10^{-6}
F0	5.82×10^3	3.02×10^{-6}
F5	4.06×10^3	2.50×10^{-6}
G0	3.57×10^3	5.97×10^{-6}
G5	2.96×10^3	7.65×10^{-6}
K0	2.71×10^3	6.88×10^{-6}
K5	2.13×10^3	1.35×10^{-5}
M0	1.55×10^3	1.50×10^{-5}
M5	6.94×10^2	3.31×10^{-5}
WD	1.97×10^3	1.05×10^{-5}
Giants	1.03×10^4	4.53×10^{-6}
Total		1.09×10^{-4}

Results: We repeat the same analysis for threatening encounter rates in the inner Galactic bulge. We assume the Kroupa (2001) initial mass function for the mass function of bulge stars through the 4-billion-year period, for the mass range of $0.1 M_\odot$ to $10 M_\odot$. A differentiation from equation 3 yields:

$$\frac{d\Gamma}{dM} = \xi(M) \langle \sigma_T \rangle_{(v)} v_*^{\text{bulge}}, \quad (13)$$

where $\xi(M)$ is the mass function of the bulge which is normalized to the stellar-mass density in the bulge with $\int \xi(M) M dM = \rho_*$, $\langle \sigma_T \rangle_{(v)}$ is the threatening cross-section, averaged over velocity and $v_*^{\text{bulge}} = 113 \text{ km/s}$ is the velocity dispersion of stars in the inner Galactic bulge (Portail et al. 2015). We note that $\langle \sigma_T \rangle_{(v)}$ also depends on the mass of encountering stars.

In the absence of velocity dispersion and number density of stars in the galactic bulge by stellar types, we used a mass-function and there is not a table of stellar types and en-

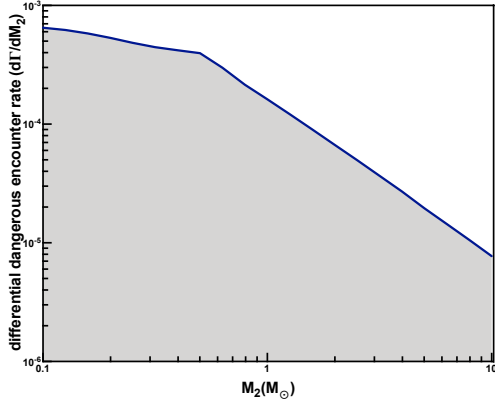


Figure 8. The differential threatening encounter rates plotted as a function of the secondary star mass in the inner region of Galactic Bulge. The integration of the differential threatening encounter rate over the secondary star mass (i.e., the gray area) portrays the total threatening encounter rate for a planet in the region.

counter rates in comparison to the solar neighborhood. The results of differential threatening encounter rate from equation (13) is shown in Figure (8). By integrating $d\Gamma/dM$ over stellar mass-function, the total threatening encounter rate is $\Gamma_{total} \approx 6.08 \times 10^{-4} \text{ Gyr}^{-1}$. This result shows that the catastrophe rate in the Galactic bulge region is about 6 times more than that of in the Solar neighborhood. Interpreting in life-evolution time, out of ≈ 400 planets in the habitable zone of solar-type stars in the inner Galactic bulge region, we expect one planet to face a threatening encounter in the hypothesized 4-billion-year period required for the evolution of advanced life.

3.3.3 Stellar environments in the Milky way galaxy and spheroidal dwarf galaxies

As noted in the past sections, Γ_T depends on the stellar number density, velocity distribution and stellar mass function. In order to calculate and compare threatening encounter rates in various stellar environments throughout the Milky way and in the spheroidal dwarf galaxies in the neighborhood, we simulated systems in a vast parameter space.

Data: The required parameters for the calculations are the stellar number density, and the velocity dispersion of stars in the environment. We assumed the same velocity distribution shape as before, and we restricted the secondary stellar mass to $1M_\odot$, in order to make the comparisons easier. Here we include the stellar environment data for the Milky way globular clusters, and Milky Way dwarf spheroidals (dSph).

The data for the Milky Way GCs come from [Baumgardt & Hilker \(2018\)](#). They acquired kinematic and structural parameters of 112 Milky Way GCs by fitting N-body simulations. We used the stellar mass-density in the cluster cores, with the velocity dispersions. We calculated the approximate envelope of the cluster parameters, and used it to show the region illustrating the overall GC populations.

The velocity dispersion and stellar number density distribution for dSph satellite galaxies is taken from [Walker et al. \(2007\)](#). Here, the full range of velocity dispersion and number density of stars is assumed and we have not taken into

account the possible relations between the distribution of the two parameters.

Results: Figure 9 shows the result and the threatening encounter rates for the stellar environments. For open clusters, the velocity dispersion is much lower than the galactic neighborhood (less than 10 km/s), therefore in the encounter rate calculations, we can neglect the rates for OC members, making them just as safe as the surrounding space [Soubiran et al. \(2018\)](#). Note that the encounter rates are independent of velocity dispersion changes in high velocities. In the velocities around 10 km/s, one can notice a turnaround; the threatening encounter rate increases with the decrease of velocity dispersion for $V_* < 10 \text{ km/s}$. This behavior can be explained by the changeover seen in figure 4, where in the high speed encounters, $b_d \propto v^{-0.5}$. If we assume a similar behavior for the threatening impact rate, then $\sigma_T \propto v^{-1}$, and therefore according to equation 3, Γ_T becomes independent of velocity. In low velocities, $b_d \propto v^{-1}$, and with the same arguments as above, $\Gamma_T \propto v^{-1}$. In the middle, the threatening impact parameter log-log slope becomes small, and therefore, $\Gamma_T \propto v^Q$, where $0 < Q < 1$, explaining the proportionality seen in Figure 9.

4 CONCLUSIONS

In this work, we studied the close stellar encounters that can disrupt the orbit of habitable planets and deprive the planets of habitability conditions. We took the parent star with the planet as a binary system while the encountering star plays the role of the third gravitating object. Using the numerical calculation for the gravitational interaction, we also considered the gravitational effect of the planet on the parent star and encountering star. In this study, we had six-dimension parameter-space for describing this encounter and studied the dependencies on the initial parameter.

The parameter space in our study had two (i) geometrical and (ii) dynamical parts. The geometric part consists of the inclination angle (i.e., i), orbital ascending node (i.e. Ω) and encountering impact parameter (i.e., b) of the planet. For the dynamical parameter space, we had the velocity and the mass of the encountering star and width of the habitable zone. We adopt the parent star and the planet similar to the Sun-Earth system, and defined a critical impact parameter to be the impact parameter which closer encounters can displace the planet from its habitable zone. Our analysis showed a power-law relationship of the critical impact-parameter with relative stellar masses of the encountering star and the parent star ($b_d \propto (M_2/M_1)^{0.34}$).

We also studied the effect of velocity of the encountering star. Our simulations showed the high-speed encounters ($v_2 \gg v_p$) have smaller critical impact parameters (comparable to the asteroid belt orbital radii), and the impact parameter decreases as $b_d \propto v_2^{-0.5}$. For most of encounters with the speed of the encountering star comparable to the speed of the planet around the primary star (i.e. $v_2 \sim v_p$), the critical impact parameter is of the order of the orbital radius of Jupiter. Also, the critical encounters with low-speed encountering stars ($v_2 \ll v_p$) require impact parameters as larger as Uranus orbital radius and the impact parameter decreases with the same rate as the velocity increases ($b_d \propto v_2^{-1}$).

Studying the dependency of critical impact parameter with habitable zone width (W_{hz}), a power-law relationship is ob-

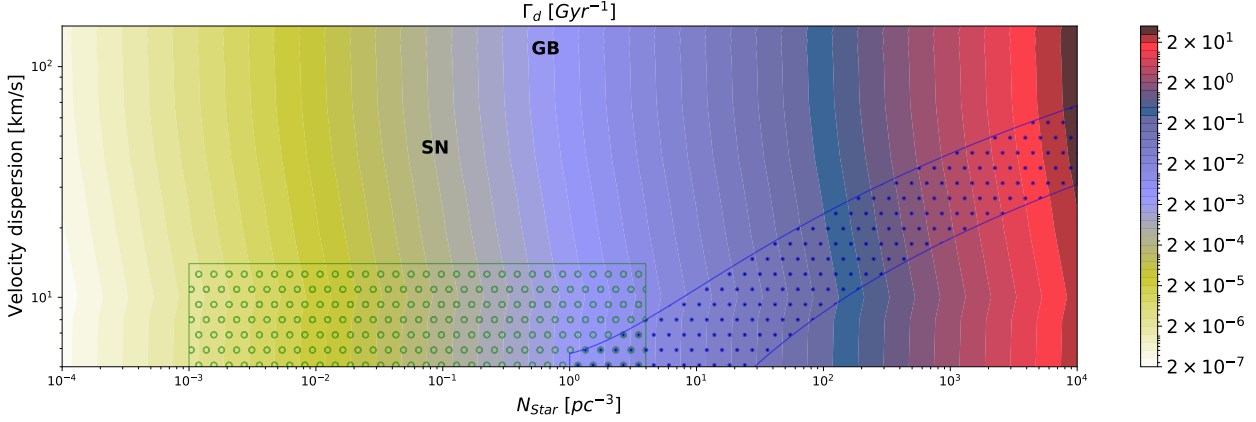


Figure 9. General threatening encounter rate (Γ_T), for general parameter spaces of stellar number density and velocity dispersion. The solar neighborhood position is shown by **SN**, and galactic bulge is shown by **GB**. The blue area with filled small dots illustrates the globular clusters, and the green rectangular area with circles shows the spheroidal dwarf galaxies surrounding Milky way. Stellar birth-clusters possess much lower velocity dispersion than the lower limits of this figure.

served, while the power depends on the velocity of the secondary star (v_2), and the stellar mass-ratio (M_2/M_1). This is an important relationship, affecting the calculations for other models for circumstellar habitable zone (we used Kasting HZ).

In order to measure the encounter rates that are able to cause an orbital change habitability hazard, we defined the threatening encounter rate (Γ_T). We reported the results for our calculations for Γ_T in different stellar environments. Our results showed that the threatening encounter rate for a planet in habitable zone around a Sun-like star is $\approx 1.09 \times 10^{-4} \text{ Gyr}^{-1}$. Therefore, in the solar neighborhood, we expect one planet out of ≈ 2300 to experience a threatening encounter in a period of 4 billion years.

We also analyzed the inner Galactic bulge region surrounding the Milky way center for the threatening encounter rates. Utilizing the number density, mass-function and velocity-dispersion of stars in the inner Galactic bulge, we estimated the $\Gamma_T \approx 6.08 \times 10^{-4} \text{ Gyr}^{-1}$. In other words, in ≈ 400 stars in the region, one experiences the threatening stellar encounter in the 4-billion-year period. Therefore, the catastrophe rate is roughly 6 times higher in the Galactic bulge compare to that in the solar neighborhood.

We extended our parameter space survey in order to calculate the threatening encounter rate for a wide set of stellar environments and included the Milky Way globular clusters and nearby spheroidal dwarf galaxies stellar number density and velocity dispersions. Concluding this work, for a planet in the habitable zone around a solar-type star, the probability of exiting planet from the habitable zone due to stellar encounter with the other stars is very low in the solar neighborhood, but in dense stellar environments, the encounter rate can be high enough to change the population of planets providing continuous habitability, despite being habitable once.

ACKNOWLEDGEMENTS

This research was supported by Sharif University of Technology Office of vice President for Research under grant no. G950214.

REFERENCES

- Abbott D. H., Isley A. E., 2002, *Earth Planet. Sci. Lett.*, 205, 53
- Allen C. W., 1973, *Astrophysical quantities*, 3rd edn. Atholone Press
- Alvarez W., 2003, *Astrobiology*, 3, 153
- Bailer-Jones C. A., 2017, *Proc. Int. Astron. Union*, 12, 144
- Bailer-Jones C. A., Rybizki J., Andrae R., Foesneau M., 2018, *Astron. Astrophys.*, 616
- Baumgardt H., Hilker M., 2018, *Mon. Not. R. Astron. Soc.*, 478, 1520
- Bobylev V., 2017, *arXiv.org*, 61, 883
- Bobylev V. V., Bajkova A. T., 2014, *Mon. Not. R. Astron. Soc.*, 441, 142
- Cai M. X., Kouwenhoven M. B. N., Zwart S. F. P., Spurzem R., 2017, *Mon. Not. R. Astron. Soc.*, 1706, arXiv:1706.03789
- Chapman C. R., Morrison D., 1994, *Nature*, 367, 33
- Clarke C. J., Pringle J. E., 1991, *Mon. Not. R. Astron. Soc.*, 249, 584
- Craig J., Krumholz M. R., 2013, *Astrophys. J.*, 769, 150
- Dodd M. S., Papineau D., Grenne T., Slack J. F., Rittner M., Pirajno F., Jonathan O., Little C. T. S., 2017, *Nature*, 543, 60
- Feng F., Bailer-Jones C. A., 2014, *Mon. Not. R. Astron. Soc.*, 442, 3653
- Fragner M. M., Nelson R. P., 2009, *Astron. Astrophys.*, 505, 873
- García-Sánchez J., Weissman P. R., Preston R. A., Jones D. L., Lestrade J.-F. F., Latham D. W., Stefanik R. P., Paredes J. M., 2001, *Astron. Astrophys.*, 379, 634
- Hall S. M., Clarke C. J., Pringle J. E., 1996, *Mon. Not. R. Astron. Soc.*, 278, 303
- Hart M. H., 1979, *Icarus*, 37, 351
- Hills J. G., 1981, *Astrophys. J.*, 86, 1730
- Hills J. G., 1984, *Astron. J.*, 89, 1559
- Howard C. D., Rich R. M., Reitzel D. B., Koch A., De Propriis R., Zhao H., 2008, *Astrophys. J.*, 688, 1060
- Hoyle F., Lyttleton R. A., 1939, *Math. Proc. Cambridge Philos. Soc.*, 35, 405

- Huang S.-S., 1959, *Publ. Astron. Soc. Pacific*, 71, 421
- Huang S.-S., 1960, *Publ. Astron. Soc. Pacific*, 72, 489
- Hurley J. R., Shara M. M., 2002, *October*, 1, 1
- Hut P., Tremaine S., 1985, 90, 1548
- Jakubík M., Neslušan L., 2008, *Contrib. Astron. Obs. Skaln. Pleso*, 38, 33
- Jiménez-Torres J. J., Pichardo B., Lake G., Throop H., 2011, *Mon. Not. R. Astron. Soc.*, 418, 1272
- Kasting J. F., Whitmire D. P., Reynolds R. T., 1993, *Icarus*, 101, 108
- Kobayashi H., Ida S., 2001, *Icarus*, 153, 416
- Kopparapu R., et al., 2013, *Astrophys. J.*, 765, 131
- Kroupa P., 2001, *Mon. Not. R. Astron. Soc.*, 322, 231
- Kunder A., et al., 2012, *Astron. J.*, 143
- Lestrade J.-F., Morey E., Lassus A., Phou N., 2011, *Astron. Astrophys.*, 532, A120
- Li G., Adams F. C., 2015, *Mon. Not. R. Astron. Soc.*, 448, 344
- Luhman K. L., Alessio P. D., Calvet N., Hartmann L., Megeath S. T., Fazio G. G., 2005, *Astrophys. J.*, pp 93–96
- Lyttleton R. A., Yabushita S., 1965, *Mon. Not. R. Astron. Soc.*, 129, 105
- Malmberg D., Davies M. B., Heggie D. C., 2011, *Mon. Not. R. Astron. Soc.*, 411, 859
- Martínez-Barbosa C. A., Jilkova L., Portegies Zwart S., Brown A. G., 2016, *Mon. Not. R. Astronomical Soc.*
- Martínez-Barbosa C. A., Jílková L., Portegies Zwart S., Brown A. G., 2017, *Mon. Not. R. Astron. Soc.*, 464, 2290
- Marzari F., Picogna G., 2013, *Astron. Astrophys.*, 550, A64
- Matese J. J., Lissauer J. J., 2002, *Icarus*, 157, 228
- Mazeeva O. A., 2004, *Sol. Syst. Res.*, 38, 325
- NASA Exoplanet Archive, [doi:10.26133/NEA1_exoplanetarchive.ipac.caltech.edu](https://doi.org/10.26133/NEA1_exoplanetarchive.ipac.caltech.edu)
- Oort J. H., 1950, *Bull. Astron. Institutes Netherlands*, 11, 91
- Ostriker E. C., 1994, *Astrophys. J.*, 424, 292
- Pandey O. P., Negi J. G., 1987, *Geophys. J. R. Astron. Soc.*, 89, 857
- Picogna G., Marzari F., 2014, *Astron. Astrophys.*, 564, A28
- Portail M., Wegg C., Gerhard O., Martínez-Valpuesta I., 2015, *Mon. Not. R. Astron. Soc.*, 448, 713
- Portegies Zwart S. F., Jílková L., 2015, *Mon. Not. R. Astron. Soc.*, 451, 144
- Rampino M. R., 2015, *Mon. Not. R. Astron. Soc.*, 448, 1816
- Rasio F. A., Ford E. B., 1996, *Science (80-)*, 274, 954
- Rein H., Liu S.-F., 2011, *Astron. Astrophys.*
- Rein H., Spiegel D. S., 2014, *Mon. Not. R. Astron. Soc.*, 446, 1424
- Rich R. M., Reitzel D. B., Howard C. D., Zhao H., 2006, *Astrophys. J.*, 688, 1060
- Rickman H., Froeschlé C., Froeschlé C., Valsecchi G. B., 2004, *Astron. Astrophys.*, 428, 673
- Rickman H., Fouchard M., Froeschlé C., Valsecchi G. B., 2008, *Celest. Mech. Dyn. Astron.*, 102, 111
- Saito R. K., et al., 2011, *Astron. Astrophys.*, 537
- Shaviv N. J., 2003, *New Astron.*, 8, 39
- Soubiran C., et al., 2018, *Astron. Astrophys.*, 619, 1
- Veras D. M., Raymond S. N., 2012, *Mon. Not. R. Astron. Soc. Lett.*, 421, 117
- Vincke K., Breslau A., Pfalzner S., 2015, *Astron. Astrophys.*, 577, A115
- Walker M., Mateo M., Olszewski E., Gnedin O., Wang X., Sen B., Woodroffe M., 2007, *Astrophys. J.*, 667, 53
- Wegg C., Gerhard O., 2013, *Mon. Not. R. Astron. Soc.*, 435, 1874
- Wickramasinghe J. T., Napier W. M., 2008, *Mon. Not. R. Astron. Soc.*, 387, 153
- Wignall P. B., 2001, *Earth Sci. Rev.*, 53, 1
- van Elteren A., et al., 2019, *Astron. Astrophys.*, 624, 1

This paper has been typeset from a $\text{\TeX}/\text{\LaTeX}$ file prepared by the author.